Photo-Fenton Reaction of Graphene Oxide: A New Strategy to Prepare Graphene Quantum Dots for DNA Cleavage

Xuejiao Zhou,[†] Yan Zhang,[†] Chong Wang,[‡] Xiaochen Wu,[†] Yongqiang Yang,[†] Bin Zheng,[‡] Haixia Wu,[†] Shouwu Guo,[†,*] and Jingyan Zhang[‡,*]

[†]National Key Laboratory of Micro/Nano Fabrication Technology, Key Laboratory for Thin Film and Microfabrication of the Ministry of Education, Research Institute of Micro/Nano Science and Technology, Shanghai Jiao Tong University, Shanghai 200240, P. R. China and [‡]School of Pharmacy, State Key Laboratory of Bioreactor Engineering, East China University of Science and Technology, Shanghai 200237, P. R. China

ABSTRACT

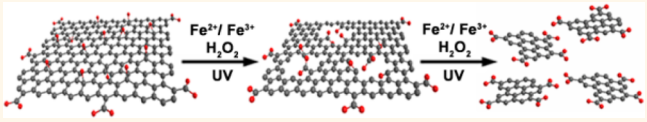

Graphene quantum dots (GQDs) are great promising in various applications owing to the quantum confinement and edge effects in addition to their intrinsic properties of graphene, but the preparation of the GQDs in bulk scale is challenging. We demonstrated in this work that the micrometer sized graphene oxide (GO) sheets could react with Fenton reagent (Fe^{2+}/Fe^{3+}/H_2O_2) efficiently under an UV irradiation, and, as a result, the GQDs with periphery carboxylic groups could be generated with mass scale production. Through a variety of techniques including atomic force microscopy, X-ray photoelectron spectroscopy, gas chromatography, ultraperformance liquid chromatography—mass spectrometry, and total organic carbon measurement, the mechanism of the photo-Fenton reaction of GO was elucidated. The photo-Fenton reaction of GO was initiated at the carbon atoms connected with the oxygen containing groups, and C—C bonds were broken subsequently, therefore, the reaction rate depends strongly on the oxidization extent of the GO. Given the simple and efficient nature of the photo-Fenton reaction of GO, this method should provide a new strategy to prepare GQDs in mass scale. As a proof-of-concept experiment, the novel DNA cleavage system using as-generated GQDs was constructed.

KEYWORDS: photo-Fenton reaction · graphene quantum dot · DNA cleavage

Besides the unique single atomic-layered structural motif and intrinsic properties of graphene,[1−6] graphene quantum dots (GQDs, the graphene sheets with lateral dimensions less than one hundred nanometers) assume numerous novel chemical/physical properties due to the quantum confinement and edge effects.[7,8] For instance, differing from the zero band gap electronic state of the graphene sheets with micrometer lateral dimension,[9] GQDs have discrete band-gaps and show typical semiconducting properties that are of great promise for many applications, such as photovoltaic devices and other optoelectronic systems.[10−13] Additionally, the photoluminescence, ultrasmall size, chemical inertia, and nontoxicity make the GQDs more suitable for cellular imaging, drug delivery, and other interfacings with biological system *in vitro* or *in vivo*.[14−17] Given the emerging properties and ongoing applications of GQDs, the preparation of GQDs has been highly demanded and several strategies have been developed so far. For examples, the hydrothermal[18] and ultrasonication breakings[17,19]of the micro-sized graphene oxide (GO) sheets, long-time chemical[20] and enzymatic oxidations of GO sheets,[21] steam etching,[22]and size fractionation techniques[23,24] have been employed for GQDs preparation. However, the harsh conditions (*e.g.*, high temperature), the time consumption (some need more than a 10 days to be performed), the low yield, and more importantly, the damage on the aromatic carbon framework are their drawbacks for mass scale manufacture. A conventional organic synthesis procedure has also been employed,[25,26] but the poor solubility and strong tendency of aggregation of the as-synthesized GQDs severely limit their practical applications. Consequently, it is still essential to develop effective strategies for the preparation of GQDs in mass scale.

The Fenton reaction was established in 1894.[27] Since then, it has been explored tremendously and has found widespread applications, especially, in the decomposition of aromatic organic pollutants in water.[28,29] Meanwhile, it has also been demonstrated

* Address correspondence to swguo@sjtu.edu.cn, jyzhang@ecust.edu.cn.

Received for review October 24, 2011 and accepted July 19, 2012.

Published online July 19, 2012
10.1021/nn301629v

that the Fenton reaction rate could be accelerated with external irradiations, such as ultraviolet (UV) light, that is called a photo-Fenton reaction.[30] From a chemistry point of view, the graphene sheets and their derivatives, such as GO sheets, could be considered as superb aromatic molecules.[1,31] In principle, they should react with the Fenton reagent.

With those thoughts in mind, the photo-Fenton reaction of GO is explored in this work. We demonstrated that GO can react with the Fenton reagent under UV irradiation, and the reaction rate depends strongly on the oxidization extent of the GO. More pronouncedly, by controlling simply on the photo-Fenton reaction conditions, the GO sheets could be converted into nanoporous graphene sheets and GQDs step wisely. The as-generated GQDs have uniform crystallinity and assume a strong photoluminescence property. The possible mechanisms of the photo-Fenton reaction of GO and the formation of GQDs were discussed. Given the simple and efficient nature of the photo-Fenton reaction of GO, this method should provide a new strategy to prepare GQDs in mass scale. Moreover, as a proof-of-concept experiment, a novel DNA cleavage system using as-generated GQDs was constructed and compared with that of the GO sheets with large lateral dimensions.

RESULTS AND DISSCUSION

GO sheets have abundant oxygen-containing groups and can be dispersed in water properly.[32] It has also been demonstrated that H_2O_2 can be dissociated into hydroxyl radicals (·OH) under the photoassisted catalysis of Fe^{3+}/Fe^{2+} in water, and as-generated ·OH has been considered as one of the most powerful oxidizing species.[29] Thus, the photo-Fenton reaction of GO sheets was carried out in an aqueous solution with pH 4 to avoid the aggregation of GO and the conversion of the iron ions to $Fe(OH)_3$ which catalytically decomposes the H_2O_2 to oxygen. The progress of the photo-Fenton reaction of GO was first monitored by atomic force microscopy (AFM) imaging. As depicted in Figure 1a,b, after 5 min of reaction, a few small holes were observed on the basal plane of GO sheets. With the reaction time increasing, more and more holes appeared on the GO sheets, and the sizes of the holes became larger. After 10 min of the reaction, there are several big holes formed, Figure 1c. The layered motif of the GO sheets is still preserved, but exhibits the porous morphology. More attractively, as illustrated in Figure 1d, after 15 min of the reaction, all GO sheets were cut into GQDs with an average lateral size of 40 nm, and thickness of ~1.2 nm (measured from the height profile of the AFM image, see Supporting Information, Figure S1) assuming the single atomic layer motif.[33,34] The GQDs powders were obtained finally after the water was removed by evaporation at 70 °C. The yield of GQDs is ~45% in weight. It is also

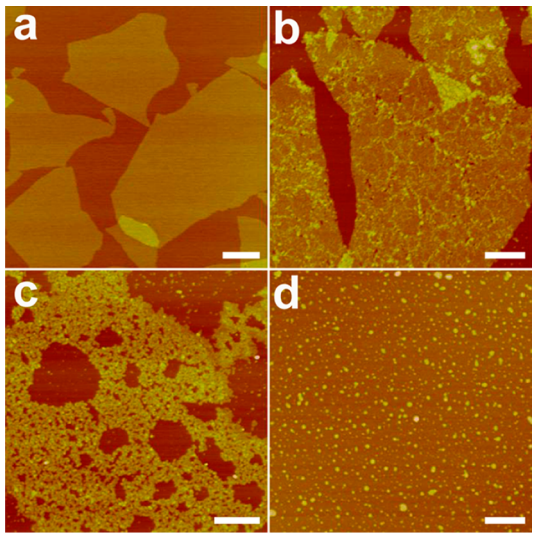

Figure 1. AFM images of GO sheets before (a), and after being reacted with the Fenton reagent under a UV irradiation (365 nm, 1000 W) for 5 (b), 10 (c), and 15 (d) min, respectively. All images were acquired under the tapping mode. All scale bars equal 500 nm.

worth noting that the as-generated GQDs can be stored in water for several months under ambient conditions (Supporting Information, Figure S2). As a control experiment, we conducted the photoreaction of the GO in water without the Fenton reagent, and found that no pitches/holes were formed on basal planes after 15 min of the reaction. Meanwhile, we tested also the reaction of the GO with the Fenton reagent under a dark condition (without the UV irradiation) for 15 min, and no pitches/holes were observed under these conditions either. The results verify that both UV light and the Fenton reagent are necessary for the photo-Fenton reaction of GO.

To get insight into the effect of the UV irradiation on the Fenton reaction of GO, the aqueous suspension of GO mixed with the Fenton reagent was exposed to a mercury lamp of 500 W for different times. As show in Supporting Information, Figure S3a, after 15 min of reaction, the morphology of GO sheets was preserved properly revealing that no reaction occurred, which is different from the results obtained with the 1000 W UV irradiation (Figure 1d). However, as shown in Figure S3b–d, under the relatively lower power (500 W) irradiation, the GO sheets can react with the Fenton reagent but at a relatively slow rate, and finally are cut into GQDs after a longer time reaction. This illustrated that the UV irradiation power plays a key role in the rate of photo-Fenton reaction of GO. The slow reaction rate is simply because the amount of ·OH generated in the reaction system is less with lower UV irradiation power. However, in the comparison of Figure 1d and Figure S3d, it should be noted that the GQDs generated under the UV irradiations with powers of 500 and 1000 W for 180 and 15 min, respectively, have almost the same size. These results imply that the sizes of GQDs could be

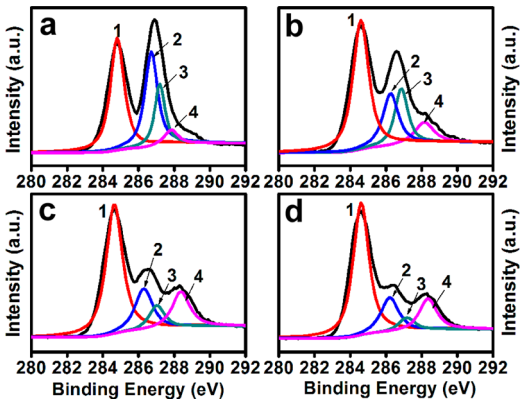

Figure 2. XPS spectra of C 1s of GO (black lines) before (a), and after the photo-Fenton reactions for 5 (b), 10 (c), and 15 (d) min. The peaks 1, 2, 3, and 4 correspond to C═C/C−C in aromatic rings, C−O (epoxy and alkoxy), C═O, and COOH groups, respectively.

controlled by varying the UV light power and photo-Fenton reaction time properly.

To follow the chemical composition variation of the GO during the photo-Fenton reaction, the XPS spectra were acquired. Figure 2 depicts the XPS spectra of C 1s of the GO before and after the photo-Fenton reaction for 5, 10, and 15 min. Before the reaction, there are four peaks at 284.5, 286.4, 287.8, and 288.5 eV, corresponding to C═C/C−C in aromatic rings, C−O (epoxy and alkoxy), C═O (carbonyl), and COOH (carboxylic) groups, respectively. With the photo-Fenton reaction processing, the intensities of C 1s XPS peaks of epoxy, alkoxy, and carbonyl groups decreased dramatically. Meanwhile, the intensity of the peak assigned to the COOH group increased gradually, implying that more COOH groups were generated during the photo-Fenton reaction. The reason might be that during the reaction more C═C and C−C bonds in GO were broken resulting in more periphery carbons, which were simultaneously oxidized into the COOH group.

To further understand the mechanism in which the carbon−carbon bonds of GO were broken through the photo-Fenton reaction to form GQDs, the photo-Fenton reaction time was elongated. Figure 3 shows the AFM images of GO reacted for 30 and 60 min (UV light, 365 nm; 1000 W). Apparently, the size of GQDs is decreasing with the reaction time increase (compare with Figure 1d), and after 60 min of reaction, no QGDs can be observed in the AFM images, indicating the further decomposition of GQDs. However disappearing in the AFM images is not an indication of the complete decomposition of GO.

To examine the species that are beyond the AFM image resolution and are generated during the photo-Fenton reaction of GO, the CO_2 content in the headspaces and total organic carbon (TOC) in the reaction solution in the quartz tubes were simultaneously analyzed using gas chromatography (GC) and ultraperformance liquid chromatography−mass spectrometry

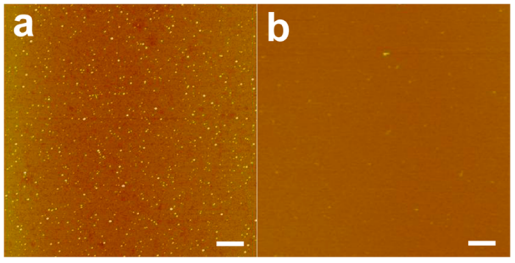

Figure 3. AFM images of GO after the photo-Fenton reactions (with UV light of 365 nm, 1000 W) for 30 (a) and 60 min (b). The scale bar equals 500 nm.

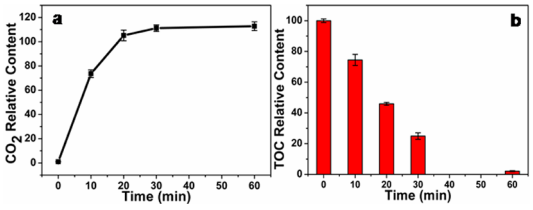

Figure 4. (a) Percentage change in the headspace CO_2 concentration of the GO with different reaction time. Zero minute corresponds to the headspace of the sample before the UV irradiation as a control (air). (b) The total organic carbon (TOC) of the reaction mixture at different reaction time. Zero minute corresponds to the reaction mixture before the photo-Fenton reaction was initiated.

(UPLC-TOF/MS), respectively. Figure 4a showed the changes of CO_2 percentage in the headspace of the reaction mixture *versus* the reaction time. As the reaction time increases, the CO_2 content increases. After 20 min of the reaction, the CO_2 content was increased more than 100%, and reached the maximum after 60 min of the reaction. The formation of CO_2 provided strong evidence that carbon−carbon bond breaking occurred during the photo-Fenton reaction of GO. At the same time, the total organic carbon (TOC) in the reaction solution dropped dramatically (Figure 4b). The decrease of TOC is consistent with the increase of CO_2 concentration in the headspace of the same reaction system suggesting that the break of the carbon−carbon bonds of GO during the photo-Fenton reaction leads to the size decrease of GO forming GQDs and CO_2 simultaneously. This implies also that in a longer reaction time, the as-generated GQDs were further converted into smaller chemical species that cannot be observed in the AFM images (Figure 3).

Figure 5 shows the UPLC and MS spectra of the reaction solutions, and the structures of some products were identified. Comparably, the majority of peaks are large molecular weight components in the solution of 15 min of reaction (Figure 5a), while in the solution of 60 min of reaction, the low molecular weight components, such as *m/z* 167 and 211, appeared, and many high molecular weight components such as *m/z* 776.2, 702.2, 610.2, 850.3, *etc.* disappeared. However, in the UPLC/MS total ion chromatogram, each peak possibly contains more than one component. To compare the

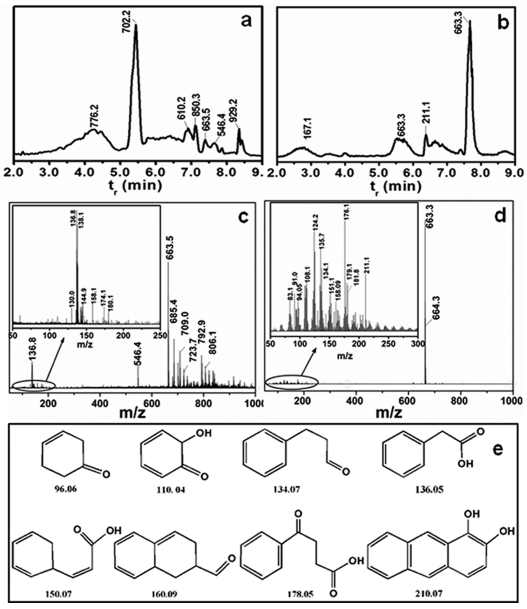

Figure 5. UPLC/MS total ion chromatogram (positive ion mode) of the samples at 15 min (a) and 60 min (b) of the reaction time. MS analysis of the two peaks with molecular weight about 663 in the samples of 15 min (c) and 60 min (d) of reaction. Insets are the blow-ups of the low molecular weight regions. (e) The structures of the products observed in spectra of panels c and d.

products of the photo-Fenton reaction of GO at different reaction times, the peak with a similar retention time and molecular weight (for instance, the major component is about *m/z* 663) in the UPLC/MS (Figure 5a,b) was further subjected to MS analysis. Figure 5 panels c and d show the MS spectra of those two samples. Obviously, after 15 min of reaction, many higher molecular components (above *m/z* 663) showed up (Figure 5c), while almost no peaks appeared above *m/z* 663 in the sample after 60 min of reaction (Figure 5d). However, in the lower molecular weight regions (insets in Figure 5d,c), a few peaks appeared after 15 min of reaction; while many species were observed after 60 min of reaction. Some of these lower molecular weight peaks were assigned to molecular ion peaks ($[M+H]^+$ in positive ion mode) of certain chemical species as shown in Figure 5e. We also performed MS analyses on the other peaks in the UPLC/MS chromatogram, and several other small molecules could be identified, but it is hard to get a complete list of the reaction products. Nevertheless, the relative percentages of the low and high molecular weight components, and the structures identified by MS in these two samples confirmed that the carbon–carbon bonds of GO and GQDs were broken through the photo-Fenton reaction forming small molecules, which is consistent with the decrease of TOC of the reaction solution and CO_2 content increase in the headspace of the reaction system (Figure 4).

On the basis of these results, we speculate that the photo-Fenton reaction of GO should be initiated at the carbon atoms connected with hydroxyl and epoxide groups, as shown schematically in Figure 6. Under the UV irradiation, a large amount of hydroxyl radical and/or peroxide radical were generated that attack the carbon atoms connected with the hydroxyl and epoxide groups to break the C–C/C=C bonds. At the same time, the newly formed oxygen-containing groups such as the quinone group or radicals that may serve further as new photo-Fenton reaction sites. Finally, the GO sheets with micrometer lateral size were cut into small fragments, even small molecules, and CO_2. Because the photo-Fenton reaction of GO is initiated at the sites with hydroxyl or epoxy groups, the small fragments will be a smaller size GO with much less or even without hydroxyl and epoxide groups, that is, a GQD (as proved by TEM and PL measurements later). Thus, preparation of GQDs with periphery carboxylic groups in mass scale under a mild condition can be realized by a simple control on the photo-Fenton reaction time.

Predictably, if the photo-Fenton reaction of GO is initiated at the carbons connected with hydroxyl and epoxide groups as proposed in Figure 6, the oxidization extent of the GO sheets should be a dominant factor to the reaction rate. To test this hypothesis, chemically reduced GOs (CRGOs) with various oxidization extents were prepared through the reduction of GO aqueous suspensions for 30, 45, and 60 min, respectively, using hydroxylamine as a reductant.[35] The as-prepared CRGOs were then mixed with Fenton reagent and exposed to a UV lamp (365 nm, 1000 W). As depicted in Supporting Information, Figure S4a, after 15 min of photo-Fenton reaction, there are only a few small holes appearing on the CRGO sheets which were reduced by hydroxylamine for 30 min. This reveals that the CRGO can react with Fenton reagent, but the reaction was much slower than that of the GO. For the CRGOs that were further reduced with hydroxylamine for 45 and 60 min, there is almost no hole or other defects that were observed on them after 15 min of photo-Fenton reaction as shown in Supporting Information, Figure S4b,c. These results confirmed unambiguously that the photo-Fenton reaction of GO should be initiated at the carbon atoms connected with the hydroxyl and epoxide groups forming GQDs with periphery carboxylic groups.

According to the aforementioned reaction mechanism, we infer that the basal plan of as-generated GQDs (shown in Figure 1d) should have defect-free two-dimensional (2D) hexagonal lattice structure closing to a pristine graphene sheet because the carbon atoms connected with the hydroxyl and epoxide groups have been removed during the photo-Fenton reaction. To verify this, the as-generated GQDs were subjected to transmission electron microscopy (TEM) measurement. Figure 7a showed the GQDs with uniform lateral dimensions of ~40 nm. As expected, the high resolution TEM image, Figure 7b, illustrates that the as-generated

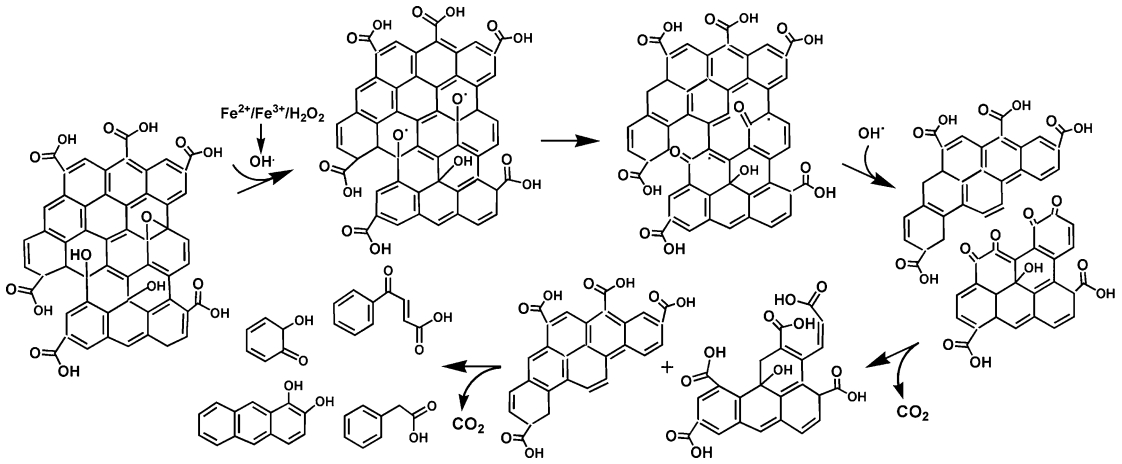

Figure 6. Schematic representation of a proposed mechanism for the photo-Fenton reaction of the GO sheets.

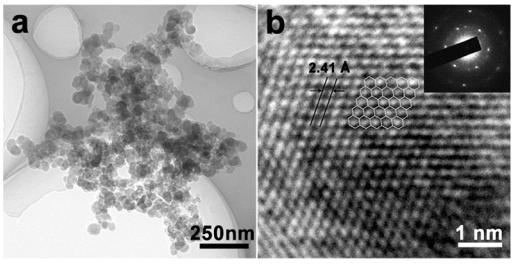

Figure 7. (a) TEM image of the as-generated GQDs. (b) HRTEM images of an individual GQD shown in panel a. Inset in panel b presents a typical electron diffraction pattern of GQD.

GQDs have 2D hexagonal symmetry crystalline structure with the in-plane lattice constant of 2.41 Å, which is comparable to that of graphite (2.46 Å).[36] This was further verified by the electron diffraction pattern of GQD, inset in Figure 7b. Additionally, the low ratio of D to G bands in the Raman spectra of GQDs also reflects their electronic conjugate statues and the 2D crystallinity of the basal plane.[37] Different from those GQDs prepared through other methods,[18−20] the G band intensity of as-generated GQDs *via* photo-Fenton reaction is stronger than that of the D band, Figure 8a, line 2 (line 1 is the spectrum of the raw GO). These results further confirm that the GQDs generated through photo-Fenton reaction of GO have a defect-free basal plane, and lead us to believe the photo-Fenton reaction takes place at the sites of the carbon atoms connected with the oxygen containing group, but not at the areas with uniform pristine graphene structures.[38,39]

The photoluminescence property of as-generated GQDs is explored as well. As shown in Figure 8b, lines 1 and 2, both raw GO sheets and GO that reacted with the Fenton reagent for 5 min (Figure 1b) are photoluminescence (PL) inactive. After 10 min of the reaction, the as-generated nanoporous GO sheets (Figure 1c) emit weak, but detectable PL (Figure 8b, line 3) using an excitation wavelength of 335 nm. The GQDs (Figure 1d) generated after 15 min of the reaction show a stronger PL

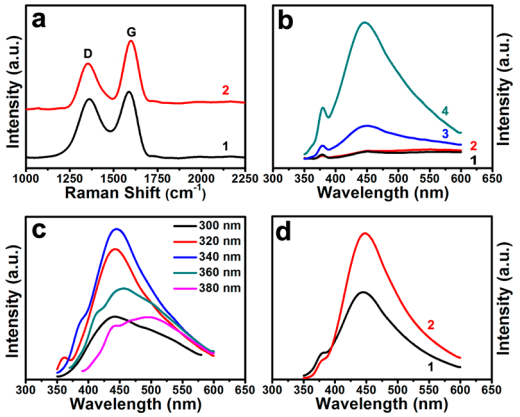

Figure 8. (a) Raman spectra of raw GO (line 1) and as-generated GQDs (line 2); (b) photoluminescence (PL) spectra of the GO aqueous suspensions before (line 1) and after the photo-Fenton reactions for 5 (line 2), 10 (line 3), and 15 (line 4) min using the excitation wavelength of 335 nm; (c) PL spectra of the aqueous suspension of GQDs (generated after 15 min of the photo-Fenton reaction) acquired using the different excitation wavelengths; (d) PL spectra of GQDs suspended in the water with pH values of 3 (line 1) and 10 (line 2).

peak centered at 450 nm, Figure 8b, line 4. Similar to other carbon nanomaterial[18,40] the PL emission wavelengths of as-generated GQDs depend strongly on the excitation wavelength as shown in Figure 8c. This implies that the GQDs might assume the same photoluminescence mechanism as other nanosized carbon materials. Most probably, both basal surface and edge defects contribute to the PL.[40] As illustrated in XPS (Figure 2d), the as-generated GQDs have plenty of periphery carboxylic groups, which may affect their PL property. To reveal this, the carboxyl groups of GQDs were converted into carboxylate groups gradually by adjusting the pH values of the GQDs suspension from 3 to 10, and their PL spectra were acquired with the same excitation (335 nm), Figure 8d. In comparison, the central peak wavelengths of the PL spectra of GQDs acquired at pH = 3 and 10 are the same, but the PL

intensity of the GQDs in suspension is much stronger with pH =10 than with pH = 3, because the negatively charged carboxylate groups, as electron donors, might be involved in the PL procedure. To further investigate the effect of periphery carboxylic groups on the PL property of GQDs, the carboxylic groups were reduced to hydroxyl groups using $LiAlH_4$ as a reductant. As illustrated in Supporting Information, Figure S5, the PL peak of as-reduced GQDs gets sharper and the intensity is relatively weaker, but its central peak wavelength is the same as that of the unreduced GQDs.

The applications of GQDs in photovoltaic devices, cellular imaging, and drug delivery have been reported.[12,16,19] To explore the applications of the as-generated GQDs, a novel DNA cleavage system was examined using the GQDs and copper ions. As shown in Figure 6, using GQDs and Cu^{2+}, about 90% supercoiled DNA was converted into nicked DNA, while using the same amount of large size GO and Cu^{2+}, only about 59% supercoiled DNA was cleaved. Although the interaction mechanism between GO and DNA is not fully understood for us yet, we previously speculated that GO intercalates into DNA.[41] However, given the large lateral size of GO relative to the diameter of DNA helix, we believe, most probably, that the GO sheet was partially intercalated in the DNA. If this is the case, the as-prepared GQDs sheets with smaller lateral size will be a better intercalator to DNA molecules than the GO sheets with micrometer lateral size. Therefore, under the same concentration, GQD/Cu^{2+} can cleave the DNA molecules more efficiently than the GO/Cu^{2+}. We previously found that about 10% of the DNA dwelled in the sample well of the agarose gel with GO/Cu^{2+} due possibly to the large size of GO that affected the movement of the DNA molecules;[41] this, however, is not observed with GQDs/Cu^{2+} suggesting that the size of GQDs is critical to their interaction with DNA (Figure 9). To further evaluate the interaction between GQDs and DNA, we explored also the cleavage activity of GQDs/Cu^{2+} to a short DNA helix (45 bp). Though the cleavage efficiency is low, some very small fragments were observed as shown in Supporting Information, Figure S6. This shows that short duplex can be unwound by GQDs. While using micrometer sized GO/Cu^{2+}, no small fragment was observed. The exploration of the detailed cleavage mechanism, optimization of cleavage conditions, and identification of the cleavage products are undergoing. Nevertheless, the results further confirmed that GQDs can interact with DNA much stronger than the micrometer-sized GO sheets. These preliminary results open further potential applications of GQDs in biological and medical research, such as cancer therapy.

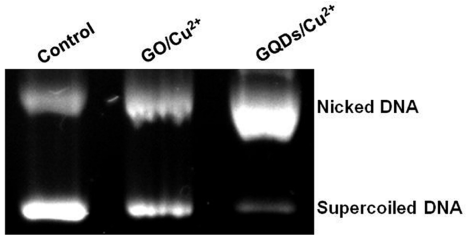

Figure 9. Agarose gel electrophoresis of GO and GQDs with Cu^{2+} incubated for 2 h at 37 °C in 50 mM Tris buffer (pH 7.2). Cu^{2+} is 10 mM, GO and GQDs are both 50 μg/mL.

CONCLUSION

In summary, we have demonstrated that the Fenton reagent could react with GO sheets readily under the UV irradiation. The reaction was initiated at the carbon atoms that connected with oxygen containing groups, and proceeds rapidly. More significantly, we envisage that the photo-Fenton reaction could be applied to the preparation of nanoporous graphene sheets and GQDs with periphery carboxylic groups in mass scale under a mild condition by a simple control of the reaction time. Moreover, the unique photo-Fenton reaction mechanism of the GO results in the formation of GQDs with a manifest crystalline state that is critical for getting high quality GQDs. The exploration of the applications of as-generated GQDs in DNA cleavage has been conducted which should open a new scope of the applications of the GQDs in biology and medicine.

METHODS

Materials. Graphite (crystalline powders, ~500 meshes) was purchased from Shanghai Yifan Graphite Co., Ltd., Shanghai, China. Sodium nitrate ($NaNO_3$), potassium permanganate ($KMnO_4$), 30% hydrogen peroxide (H_2O_2), ferric chloride ($FeCl_3 \cdot 6H_2O$), $LiAlH_4$, and hydroxylamine hydrochloride ($NH_2OH \cdot HCl$) were obtained from Sinopharm Chemical Reagent Co., Ltd., Shanghai, China. Concentrated H_2SO_4 and HCl were acquired from Shanghai Lingfeng Chemical Reagent Co., Ltd., Shanghai, China. All of the reagents were used as received.

Photo-Fenton Reaction of GO. GO and CRGOs were generated as described in our previous work.[35] The photo-Fenton reactions of GO and CRGOs were carried out in a photoreactor equipped with the irradiation lamps having different emission wavelengths and powers (Bilon, Shanghai). The reaction is carried out under vigorous stirring in a 40 mL quartz tube which is installed 6 cm away from the irradiation lamp. The lamps were equipped inside a cylindrical Pyrex tube cooled by circulated water. In a typical experiment, 5 mL of 0.5 mg/mL GO aqueous suspension, 20 mL of 20 mM H_2O_2, and 100 μL of 1.0 mM of $FeCl_3$ were mixed in a quartz tube under vigorous stirring. The pH of the mixture was adjusted to 4. The reaction was initiated by exposing the quartz tube to a mercury lamp (365 nm, 1000 W). The reaction products were dialyzed in ultrapure water for 2 days to remove iron ions, trace H_2O_2, and other small molecular reaction products. To get insight into the effect of periphery carboxylic groups on the PL properties, the as-generated GQDs were reduced for 4.5 h in dried tetrahydrofuran using $LiAlH_4$ as a reductant to convert the carboxylic groups to hydroxyl.

Instrumentations. AFM images were acquired using a Multimode Nanoscope V scanning probe microscopy system (Bruker, USA). The commercially available AFM cantilever tips with a

force constant of ~50 N/m and resonance vibration frequency of ~350 kHz (Bruker, USA) were used. The specimens were prepared by solution casting the aqueous suspensions of GO or GQDs on a freshly cleaved mica surface and drying in air. TEM images were obtained using a JEM-2010 transmission electron microscope (JEOL, Japan) operated at 200 kV. The samples were prepared by placing the aqueous suspension of GQDs after the dialysis on the copper grids and drying under ambient condition. XPS measurements were performed on an Axis Ultra DLD spectrometer (Kratos Analytical, UK) using a monochromated Al Kα source at 15 kV. Raman spectra were recorded on an Invia/Reflrx Lasser micro-Raman spectroscope (Renishaw, England) with 514 nm excitation wavelength of laser. Samples for Raman spectroscopy were prepared by dropping the aqueous suspension of GO or GQDs on the surface of freshly cleaved mica and drying under ambient condition. The FT-IR spectra were acquired on a EQUINOX 55 FT-IR spectrometer (Bruker, Germany). The specimens for FT-IR measurement were prepared by grinding the dried powder of GQDs or GO with KBr together, and then compressing into thin pellets. LC-HRMS was performed on a Waters ACQUITY UPLC system equipped with a binary solvent delivery manager and a sample manager, coupled with a Waters Micromass Q-TOF Premier mass spectrometer equipped with an electrospray interface (Waters Corporation, Milford, MA) at the Instrumental Analysis Center of Shanghai Jiao Tong University. An aliquot of 3 μL of reaction solution was injected into a BEH C18 column (100 mm $\times$ 2.1 mm, 1.7 μm) maintained at 45 °C. The column was eluted with gradient solvent from A:B (10:90) to A:B (0:100) at a flow rate of 0.40 mL/min, where A is acetonitrile (0.1% (v/v) formic acid) and B is aqueous formic acid (0.1% (v/v) formic acid). The full scan data was acquired from m/z 50−1000 with a 0.3 s scan time, using a capillary voltage of 3.0 kV for the positive ion mode. To identify the small fragments, the reaction mixtures after 15 and 60 min of reactions were selectively subjected to UPLC-TOF-MS measurements. Total organic carbon of the samples was determined with a Multi N/C 3000 instrument (Germany AJ). GC samples were carried out with GC-14B instrument (Shimadzu, Japan). For the GC analysis, the quartz tube was capped with a septum and parafilm leaving enough headspace for sampling with a gastight needle. The identification of CO_2 was based on the standard sample. CO_2 concentrations were evaluated relative to ambient N_2 concentration present in the headspace before the reaction was initiated by UV light irradiation. Agarose gel electrophoresis was performed as we previously described.[41] The PL spectra were obtained on a Hitachi F-4600 instrument. The pH of samples was tuned by ammonia and acetic acid. In the emission spectrum, the detection wavelength is 450 nm and excitation wavelength is 335 nm.

Conflict of Interest: The authors declare no competing financial interest.

Supporting Information Available: Detailed supplementary data as described in the text. This material is available free of charge *via* the Internet at http://pubs.acs.org.

Acknowledgment. This work was supported by the NSFC (Nos. 91123011, 90923041, 31070742), the National "973 Program" (No. 2010CB933900), and the State Key Laboratory of Bioreactor Engineering (No. 2060204) of China.

REFERENCES AND NOTES

1. Geim, A. K.; Novoselov, K. S. The Rise of Graphene. *Nat. Mater.* **2007**, *6*, 183–191.
2. Zhu, Y.; Murali, S.; Cai, W.; Li, X.; Suk, J. W.; Potts, J. R.; Ruoff, R. S. Graphene and Graphene Oxide: Synthesis, Properties, and Applications. *Adv. Mater.* **2010**, *22*, 3906–3924.
3. Li, X.; Wang, X.; Zhang, L.; Lee, S.; Dai, H. Chemically Derived, Ultrasmooth Graphene Nanoribbon Semiconductors. *Science* **2008**, *319*, 1229–1232.
4. Li, D.; Müller, M. B.; Gilje, S.; Kaner, R. B.; Wallace, G. G. Processable Aqueous Dispersions of Graphene Nanosheets. *Nat. Nanotechnol.* **2008**, *3*, 101–105.
5. Stankovich, S.; Dikin, D. A.; Dommett, G. H. B.; Kohlhaas, K. M.; Zimney, E. J.; Stach, E. A.; Piner, R. D.; Nguyen, S. T.; Ruoff, R. S. Graphene-Based Composite Materials. *Nature* **2006**, *442*, 282–286.
6. Huang, X.; Yin, Z.; Wu, S.; Qi, X.; He, Q.; Zhang, Q.; Yan, Q.; Boey, F.; Zhang, H. Graphene-Based Materials: Synthesis, Characterization, Properties, and Applications. *Small* **2011**, *7*, 1876–1902.
7. Girit, C. O.; Meyer, J. C.; Erni, R.; Rossell, M. D.; Kisielowski, C.; Yang, L.; Park, C. H.; Crommie, M. F.; Cohen, M. L.; Louie, S. G.; Zetti, A. Graphene at the Edge-Stability and Dynamics. *Science* **2009**, *323*, 1705–1708.
8. Ponomarenko, L. A.; Schedin, F.; Katsnelson, M. I.; Yang, R.; Hill, E. W.; Novoselov, K. S.; Geim, A. K. Chaotic Dirac Billiard in Graphene Quantum Dots. *Science* **2008**, *320*, 356–358.
9. Han, M. Y.; Özyilmaz, B.; Zhang, Y.; Kim, P. Energy Band-Gap Engineering of Graphene Nanoribbons. *Phys. Rev. Lett.* **2007**, *98*, 206805.
10. Li, Y.; Hu, Y.; Zhao, Y.; Shi, G.; Deng, L.; Hou, Y.; Qu, L. An Electrochemical Avenue to Green-Luminescent Graphene Quantum Dots as Potential Electron-Acceptors for Photovoltaics. *Adv. Mater.* **2011**, *23*, 776–780.
11. Yan, X.; Cui, X.; Li, B.; Li, L. Large, Solution-Processable Graphene Quantum Dots as Light Absorbers for Photovoltaics. *Nano Lett.* **2010**, *10*, 1869–1873.
12. Ritter, K. A.; Lyding, J. W. The Influence of Edge Structure on the Electronic Properties of Graphene Quantum Dots and Nanoribbons. *Nat. Mater.* **2009**, *8*, 235–242.
13. Wu, J.; Pisula, W.; Mullen, K. Graphenes as Potential Material for Electronics. *Chem. Rev.* **2007**, *107*, 718–747.
14. Yang, K.; Zhang, S.; Zhang, G.; Sun, X.; Lee, S.-T.; Liu, Z. Graphene in Mice: Ultrahigh *in Vivo* Tumor Uptake and Efficient Photothermal Therapy. *Nano Lett.* **2010**, *10*, 3318–3323.
15. Liu, Z.; Robinson, J. T.; Sun, X.; Dai, H. PEGylated Nanographene Oxide for Delivery of Water-Insoluble Cancer Drugs. *J. Am. Chem. Soc.* **2008**, *130*, 10876–10877.
16. Zhu, S.; Zhang, J.; Qiao, C.; Tang, S.; Li, Y.; Yuan, W.; Li, B.; Tian, L.; Liu, F.; Hu, R.; *et al.* Strongly Green-Photoluminescent Graphene Quantum Dots for Bioimaging Applications. *Chem. Commun.* **2011**, *47*, 6858.
17. Robinson, J. T.; Tabakman, S. M.; Liang, Y.; Wang, H.; Casalongue, H. S.; Vinh, D.; Dai, H. Ultrasmall Reduced Graphene Oxide with High Near-Infrared Absorbance for Photothermal Therapy. *J. Am. Chem. Soc.* **2011**, *133*, 6825–6831.
18. Pan, D.; Zhang, J.; Li, Z.; Wu, M. Hydrothermal Route for Cutting Graphene Sheets into Blue-Luminescent Graphene Quantum Dots. *Adv. Mater.* **2010**, *22*, 734–738.
19. Sun, X.; Liu, Z.; Welsher, K.; Robinson, J. T.; Goodwin, A.; Zaric, S.; Dai, H. Nano-graphene Oxide for Cellular Imaging and Drug Delivery. *Nano Res.* **2008**, *1*, 203–212.
20. Zhang, L.; Liang, J.; Huang, Y.; Ma, Y.; Wang, Y.; Chen, Y. Size-Controlled Synthesis of Graphene Oxide Sheets on a Large Scale Using Chemical Exfoliation. *Carbon* **2009**, *47*, 3365–3368.
21. Kotchey, G. P.; Allen, B. L.; Vedala, H.; Yanamala, N.; Kapralov, A. A.; Tyurina, Y. Y.; Klein-Seetharaman, J.; Kagan, V. E.; Star, A. The Enzymatic Oxidation of Graphene Oxide. *ACS Nano* **2011**, *5*, 2098–2108.
22. Han, T. H.; Huang, Y. K.; Tan, A. T. L.; Dravid, V. P.; Huang, J. Steam Etched Porous Graphene Oxide Network for Chemical Sensing. *J. Am. Chem. Soc.* **2011**, *133*, 15264–15267.
23. Sun, X.; Luo, D.; Liu, J.; Evans, D. G. Monodisperse Chemically Modified Graphene Obtained by Density Gradient Ultracentrifugal Rate Separation. *ACS Nano* **2010**, *4*, 3381–3389.
24. Wang, X.; Bai, H.; Shi, G. Size Fractionation of Graphene Oxide Sheets by pH-Assisted Selective Sedimentation. *J. Am. Chem. Soc.* **2011**, *133*, 6338–6342.
25. Wu, J.; Tomovic, Z.; Enkelmann, V.; Mullen, K. From Branched Hydrocarbon Propellers to C3-Symmetric Graphite Disks. *J. Org. Chem.* **2004**, *69*, 5179–5186.
26. Yan, X.; Cui, X.; Li, L. Synthesis of Large, Stable Colloidal Graphene Quantum Dots with Tunable Size. *J. Am. Chem. Soc.* **2010**, *132*, 5944–5945.
27. Fenton, H. J. H. Oxidation of Tartaric Acid in the Presence of Iron. *J. Chem. Soc.* **1894**, *65*, 899–910.

28. Cheng, M.; Ma, W.; Li, J.; Huang, Y.; Zhao, J. Visible-Light-Assisted Degradation of Dye Pollutants over Fe(III)-Loaded Resin in the Presence of H_2O_2 at Neutral pH Values. *Environ. Sci. Technol.* **2004**, *38*, 1569–1575.
29. Ikehata, K.; El-Din, M. G. Aqueous Pesticide Degradation by Hydrogen Peroxide/Ultraviolet Irradiation and Fenton-type Advanced Oxidation Processes: A Review. *J. Environ. Eng. Sci.* **2006**, *5*, 81–135.
30. Bauer, R.; Fallmann, H. The Photo-Fenton Oxidation -A Cheap and Efficient Wastewater Treatment Method. *Res. Chem. Intermed.* **1997**, *23*, 341–354.
31. Erickson, K.; Erni, R.; Lee, Z.; Alem, N.; Gannett, W.; Zettl, A. Determination of the Local Chemical Structure of Graphene Oxide and Reduced Graphene Oxide. *Adv. Mater.* **2010**, *22*, 4467–4472.
32. Dreyer, D. R.; Park, S.; Bielawski, C. W.; Ruoff, R. S. The Chemistry of Graphene Oxide. *Chem. Soc. Rev.* **2010**, *39*, 228–240.
33. Zhang, J.; Yang, H.; Shen, G.; Cheng, P.; Zhang, J.; Guo, S. Reduction of Graphene Oxide *via* Ascorbic Acid. *Chem. Commun.* **2010**, *46*, 1112.
34. Park, S.; Ruoff, R. S. Chemical Methods for the Production of Graphenes. *Nat. Nanotechnol.* **2009**, *4*, 217–224.
35. Zhou, X.; Zhang, J.; Wu, H.; Yang, H.; Zhang, J.; Guo, S. Reducing Graphene Oxide *via* Hydroxylamine: A Simple and Efficient Route to Graphene. *J. Phys. Chem. C* **2011**, *115*, 11957–11961.
36. Baskin, Y.; Meyer, L. Lattice Constants of Graphite at Low Temperatures. *Phys. Rev.* **1955**, *100*, 544.
37. Reich, S.; Thomsen, C. Raman Spectroscopy of Graphite. *Phil. Trans. R. Soc. London A* **2004**, *362*, 2271–2288.
38. Solis-Fernández, P.; Paredes, J. I.; Villar-Rodil, S.; Guardia, L.; Fernández-Merino, M. J.; Dobrik, G.; Biró, L. P.; Martínez-Alonso, A.; Tascón, J. M. D. Global and Local Oxidation Behavior of Reduced Graphene Oxide. *J. Phys. Chem. C* **2011**, *115*, 7956–7966.
39. Matsumoto, Y.; Koinuma, M.; Ida, S.; Hayami, S.; Taniguchi, T.; Hatakeyama, K.; Tateishi, H.; Watanabe, Y.; Amano, S. Photoreaction of Graphene Oxide Nanosheets in Water. *J. Phys. Chem. C* **2011**, *115*, 19280–19286.
40. Baker, S. N.; Baker, G. A. Luminescent Carbon Nanodots: Emergent Nanolights. *Angew. Chem., Int. Ed.* **2010**, *49*, 6726–6744.
41. Ren, H.; Wang, C.; Zhang, J.; Zhou, X.; Xu, D.; Zheng, J.; Guo, S.; Zhang, J. DNA Cleavage System of Nanosized Graphene Oxide Sheets and Copper Ions. *ACS Nano* **2010**, *4*, 7169–7174.